Zmpste24 deficiency in mice causes spontaneous bone fractures, muscle weakness, and a prelamin A processing defect

Martin O. Bergo*†‡, Bryant Gavino*, Jed Ross§, Walter K. Schmidt¶, Christine Hong*, Lonnie V. Kendall‖, Andreas Mohr**, Margarita Meta**, Harry Genant**, Yebin Jiang**, Erik R. Wisner‖, Nicholas van Bruggen§, Richard A. D. Carano§, Susan Michaelis¶, Stephen M. Griffey‖, and Stephen G. Young*†,††

*Gladstone Institute of Cardiovascular Disease, University of California, San Francisco, CA 94141-9100; †Cardiovascular Research Institute, University of California, San Francisco, CA 94143; §Genentech, Incorporated, South San Francisco, CA 94080; ¶Department of Cell Biology, The Johns Hopkins University School of Medicine, Baltimore, MD 21205; ‖Comparative Pathology Laboratory, University of California, Davis, CA 95616; **Department of Radiology, University of California, San Francisco, CA 94143; and ††Department of Medicine, University of California, and the Medical Services, San Francisco General Hospital, San Francisco, CA 94110

Communicated by Richard J. Havel, University of California, San Francisco, CA, August 1, 2002 (received for review June 26, 2002)

Zmpste24 is an integral membrane metalloproteinase of the endoplasmic reticulum. Biochemical studies of tissues from *Zmpste24*-deficient mice (*Zmpste24*$^{-/-}$) have indicated a role for Zmpste24 in the processing of *CAAX*-type prenylated proteins. Here, we report the pathologic consequences of *Zmpste24* deficiency in mice. *Zmpste24*$^{-/-}$ mice gain weight slowly, appear malnourished, and exhibit progressive hair loss. The most striking pathologic phenotype is multiple spontaneous bone fractures—akin to those occurring in mouse models of osteogenesis imperfecta. Cortical and trabecular bone volumes are significantly reduced in *Zmpste24*$^{-/-}$ mice. *Zmpste24*$^{-/-}$ mice also manifested muscle weakness in the lower and upper extremities, resembling mice lacking the farnesylated *CAAX* protein prelamin A. Prelamin A processing was defective both in fibroblasts lacking *Zmpste24* and in fibroblasts lacking the *CAAX* carboxyl methyltransferase Icmt but was normal in fibroblasts lacking the *CAAX* endoprotease Rce1. Muscle weakness in *Zmpste24*$^{-/-}$ mice can be reasonably ascribed to defective processing of prelamin A, but the brittle bone phenotype suggests a broader role for Zmpste24 in mammalian biology.

metalloproteinase | knockout mice | brittle bones | CAAX motif

The mammalian zinc metalloproteinase Zmpste24 has attracted attention because it shares a high degree of sequence identity with Ste24p, a *Saccharomyces cerevisiae* enzyme required for the maturation of the farnesylated mating pheromone a-factor (1–3). Ste24p plays two distinct roles in a-factor biogenesis (2, 4). First, it acts as a *CAAX* endoprotease, clipping off the C-terminal three amino acids from the protein (i.e., the *−AAX* of the *CAAX* motif) (3). Release of the *−AAX* from a-factor can also be mediated by Rce1p, the *CAAX* endoprotease involved in Ras processing (3). The removal of the *−AAX* exposes a carboxyl-terminal farnesylcysteine, which is methylated by Ste14p (5). Second, Ste24p clips the amino-terminal extension of a-factor, rendering it susceptible to a final endoproteolytic cleavage by Axl1p or Ste23p (6). Aside from a-factor, no other substrates for Ste24p have been identified, but other substrates likely exist because genetic screens in yeast have demonstrated that *STE24* mutations can reverse the topological orientation of membrane proteins (7) and can affect the viability of yeast with mutations in genes encoding actin cytoskeleton proteins (8).

Zmpste24 faithfully carries out both of Ste24p's processing steps in a-factor biogenesis and thus is a *bona fide* Ste24p ortholog (2, 9). Although it would be tempting to speculate that *Zmpste24* processes an "a-factor-like" peptide in mammals, no a-factor ortholog has yet been identified. We have previously speculated that prelamin A (a precursor to lamin A, a component of the nuclear lamina) might be a Zmpste24 substrate (2, 6) because prelamin A (like yeast a-factor) is a farnesylated *CAAX* protein that undergoes more than one proteolytic processing step (10). After the removal of the C-terminal *−AAX*, an additional 15 residues are removed from the C terminus of the protein, generating mature lamin A (10).

Three years ago, to assess the importance of *Zmpste24* in mammals, we produced *Zmpste24* knockout mice (*Zmpste24*$^{-/-}$) by replacing the exon encoding the zinc-binding domain with a neomycin resistance cassette (*neo*) (9). We reported biochemical studies showing that tissues and cells lacking *Zmpste24* were deficient in their ability to carry out the N- and C-terminal proteolytic processing steps in a-factor biogenesis. Although obvious abnormalities (including muscle weakness and spontaneous bone fractures) were plainly evident in independently derived lines of knockout mice, we were reluctant to report those data with the biochemical studies (9) because we were concerned that one or more of the phenotypes could have been due to effects of the *neo* cassette (particularly its promoter and enhancer elements) on the transcription of neighboring genes (11). Accordingly, we proceeded with the characterization of *Zmpste24*$^{-/-}$ mice lacking the *neo* cassette. In May 2002, Pendás *et al.* (12) reported a second mutant *Zmpste24* allele in which several exons were replaced by a *neo* cassette. They reported that *Zmpste24* deficiency was associated with a prelamin A processing defect as well as partial lipodystrophy, muscular dystrophy, and cardiomyopathy.

Here, we report the pathologic findings in *Zmpste24*-deficient mice, document a prelamin A processing defect in *Zmpste24*-deficient tissues and fibroblasts, and show that the prelamin A processing defect also occurs in cells lacking Icmt, the enzyme that carries out the carboxyl methylation of prenylated proteins.

Materials and Methods

***Zmpste24*$^{-/-}$ Mice.** Mice from two embryonic stem cell lines, each with a single integration event, were studied (9). *Zmpste24*$^{-/-}$ mice lacking the *neo* were generated by excising the *neo* with a deleter-*Cre* mouse strain (13). The phenotypes of the *neo*-positive and "*neo*-less" *Zmpste24*$^{-/-}$ mice were compared over a 2-year time frame. The mice had a mixed genetic background (≈50% C57BL/6 and ≈50% 129/SvJae), were fed a mouse chow diet, and were housed in a virus-free barrier facility.

Pathological Examination. Full necropsies were performed on 16-, 20-, and 24-week-old *Zmpste24*$^{-/-}$ mice and littermate controls (n = 3–7) with histologic examination of >30 tissues, including all regions of the skeleton. In addition, necropsies and routine

Abbreviation: μCT, microcomputed tomography.

‡To whom reprint requests should be addressed. E-mail: mbergo@gladstone.ucsf.edu.

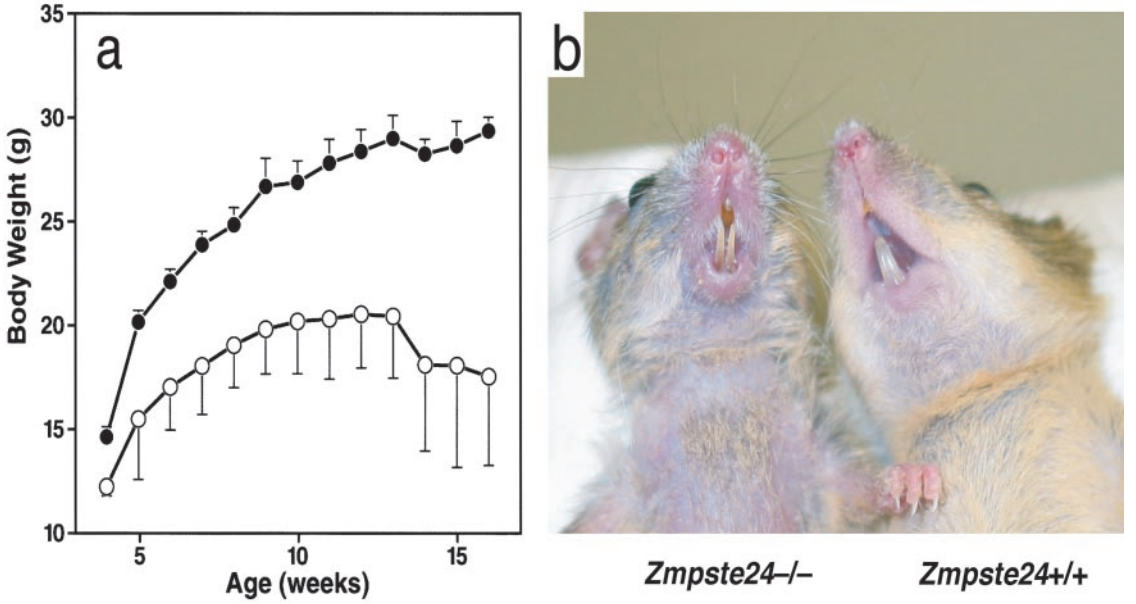

Fig. 1. (*a*) Retarded growth in male *Zmpste24*$^{-/-}$ mice ($n = 4$) vs. littermate male *Zmpste24*$^{+/+}$ mice ($n = 13$). Similar results were obtained with female mice (not shown). (*b*) Photograph of a 3-month-old *Zmpste24*$^{-/-}$ mouse and littermate *Zmpste24*$^{+/+}$ mouse.

histology of the musculoskeletal system were performed on mice at 3, 6, 9, 16, 20, 24, and 30 weeks of age ($n = 4–8$). Whole-body radiographs were performed on 6- to 30-week-old *Zmpste24*$^{-/-}$ mice and littermate controls ($n = 31$) with a Faxitron specimen radiography system (Wheeling, IL).

Prelamin A Processing. Extracts from *Zmpste24*$^{+/+}$ fibroblasts, *Zmpste24*$^{-/-}$ fibroblasts, *Rce1*$^{-/-}$ fibroblasts (14), *Icmt*$^{-/-}$ fibroblasts (15), and wild-type fibroblasts treated with a farnesyltransferase inhibitor (SCH66336) were size-fractionated on SDS/4–15% polyacrylamide gels, and Western blots were performed with a C-terminal antilamin A goat antibody (sc-6214, Santa Cruz Biotechnology) and an N-terminal anti-lamin A/C mouse monoclonal antibody (sc-7293, Santa Cruz Biotechnology).

Microcomputed Tomography (μCT) Scans. *Zmpste24*$^{-/-}$ mice ($n = 3–5$) were examined with a MicroCT 40 scanner (Scanco Medical, Bassersdorf, Switzerland) at 18 days, 2 months, and 3 months of age. The μCT scanner allows for imaging and quantification of cancellous bone microstructure, in both two and three dimensions. The sample was scanned in the axial plane mounted in a cylindrical sample holder with a current of 0.16 mA, a voltage of 50 kV, at an isotropic resolution of 20 μm (image matrix 1024 $\times$ 1024 pixels). Images of *Zmpste24*$^{+/+}$ and *Zmpste24*$^{-/-}$ bones were generated at the identical threshold.

The three-dimensional trabecular structure of the 12th thoracic vertebral body was constructed with the internal software of the μCT system. Cortical bone and trabecular bone were manually separated on each slice by a cursor line. Several structural parameters, including the bone volume to total volume ratio and trabecular thickness, were measured. The central 50% (the diaphysis) of the tibia and fibula were also analyzed. The cortical bone volume and density were determined by application of an automated image segmentation algorithm and image analysis software libraries (AnalyzeDirect, Lenexa, KS). Histogram analysis and morphological filtering were used to extract the cortex volume and total tibia/fibula volume. A cortical bone threshold (0.77 gHA/cm^3) was determined by histogram analysis of the data. The threshold was applied to extract cortex voxels in the image data. A series of morphological operations within the software package was then applied to link cortex voxels and remove voxels of similar density within trabeculae. The ratio of cortical bone volume to total diaphyseal volume and the cortical bone density were calculated.

Results and Discussion

***Zmpste24*$^{-/-}$ Mice.** The phenotypes of *neo*-positive and *neo*-less knockout mice were identical over a 2-year period of study. Heterozygotes (*Zmpste24*$^{+/-}$) appear normal for the first 12 months of life, but by 15 months of age, most heterozygotes were smaller than wild-type (*Zmpste24*$^{+/+}$) littermates, appeared weak, and lost hair. *Zmpste24*$^{-/-}$ mice weigh slightly less than their littermates at weaning (3 weeks of age) and gain weight slowly (Fig. 1*a*). The mice also manifest muscle weakness (described below). By 6–8 weeks of age, they develop kyphosis of the spine, lose hair, and appear very malnourished. These phenotypes were progressive, and the mice either died or were killed by 6–7 months of age.

Spontaneous Bone Fractures. The lower incisors of *Zmpste24*$^{-/-}$ mice were splayed apart, thin, and long (Fig. 1*b*). This peculiar phenotype has been noted previously in a mouse model of osteogenesis imperfecta (16). Osteogenesis imperfecta in humans is characterized by brittle bones (17), and transgenic and gene-targeted mouse models of this disease develop spontaneous bone fractures (18–20). The incisor abnormalities in *Zmpste24*$^{-/-}$ mice led us to predict that the *Zmpste24*$^{-/-}$ mice might develop spontaneous bone fractures. Indeed, this proved to be the case. By 24–30 weeks of age, nearly every rib in *Zmpste24*$^{-/-}$ mice was broken in the vicinity of the costovertebral junction—obvious from hypertrophic calluses at the fracture sites (Fig. 2*a*). Callus surrounding broken ribs was also visible by routine x rays (Fig. 2*b*) and surface renderings of the vertebral spine from μCT scans (Fig. 2*c*). Penetrating views of the vertebral spine from the μCT scans (maximal intensity projections) revealed fractures of the tips of most ribs (Fig. 2*d*).

Microscopic sections also revealed broken ribs surrounded by exuberant fibrous tissue (Fig. 2 *e* and *f*). The fracture sites were surprisingly acellular, with little inflammatory infiltrate and minimal evidence of healing. Bone fragments within fracture

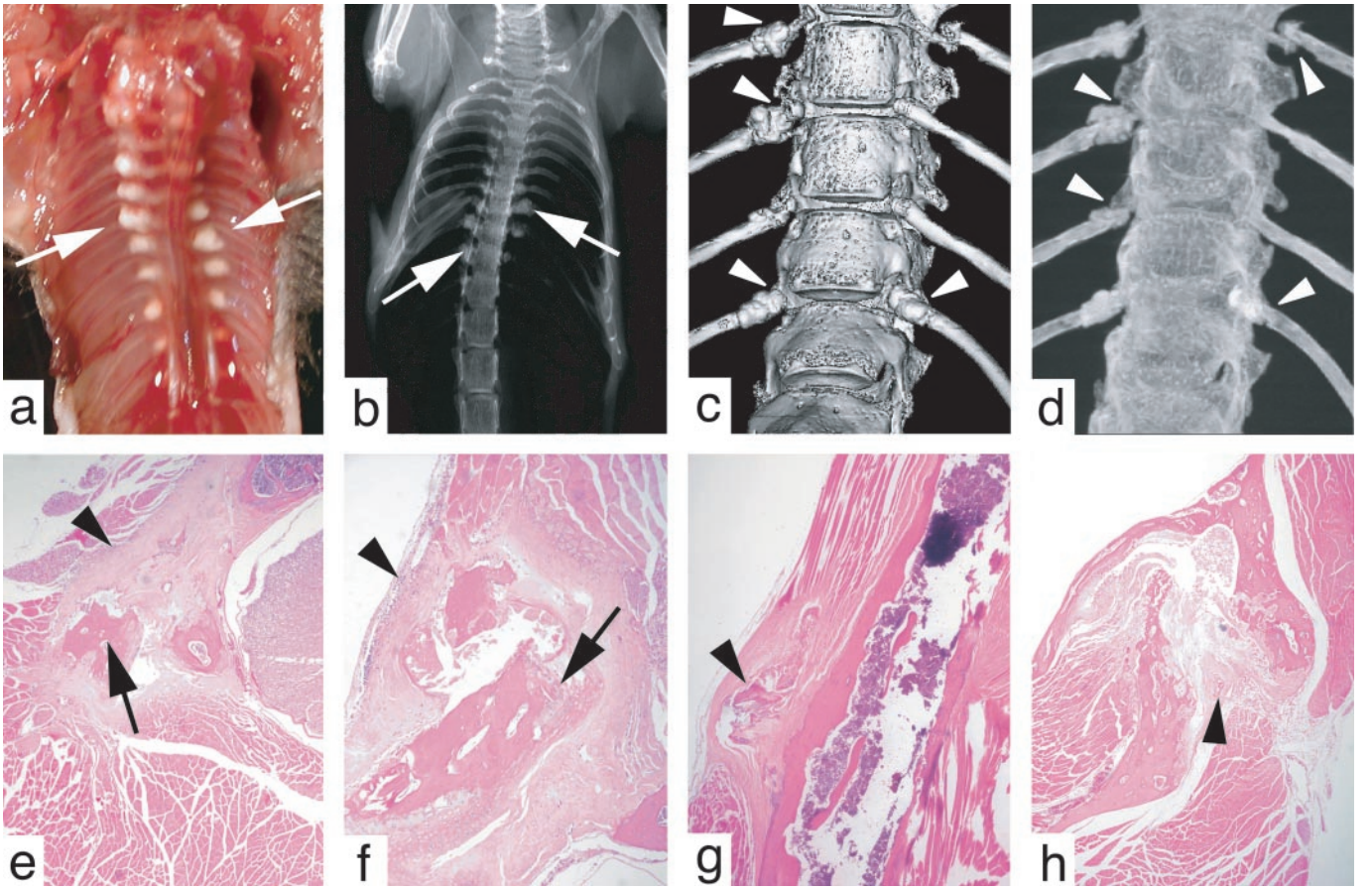

Fig. 2. (*a*) Thorax of a 24-week-old *Zmpste24*$^{-/-}$ mouse. Fibrotic lesions surrounding broken ribs are indicated by arrows. (*b*) Radiograph of a *Zmpste24*$^{-/-}$ mouse, revealing callus formation surrounding rib fractures (arrows). (*c*) Surface rendering of a μCT scan of the lower thoracic spine of a *Zmpste24*$^{-/-}$ mouse. Callus is visible at the tips of several ribs near the costovertebral joints (arrowheads). (*d*) Maximal intensity projection from a μCT scan of the lower thoracic spine of a *Zmpste24*$^{-/-}$ mouse, revealing multiple rib fractures (arrowheads). (*e* and *f*) Hematoxylin- and eosin-stained sections of rib fractures (arrows) and surrounding fibrosis (arrowheads). (*g*) Avulsion of a fragment of bone (arrowhead) from the cortex of the humerus. (*h*) Fracture of the mandible with fibrosis between bone fragments (arrowhead).

sites were frequently necrotic, lacking viable osteocytes. *Zmpste24*$^{-/-}$ mice manifested bone fractures in multiple locations aside from the ribs, including the scapula, clavicle, sternum, zygomatic arch, mandible, and humerus. The avulsion of a fragment of bone from the humerus of a 24-week-old *Zmpste24*$^{-/-}$ mouse is shown in Fig. 2*g*, and a fracture of the mandible in a 24-week-old *Zmpste24*$^{-/-}$ mouse is shown in Fig. 2*h*. The epiphyseal plates of the large bones of the upper and lower extremities were invariably normal (not shown).

By 8 weeks of age, *Zmpste24*$^{-/-}$ mice invariably ($n = 8$ examined) had fractures of the posterior portion of the zygomatic arch where the masseter originates (Fig. 3 *a–d*). These fractures did not heal, and the posterior portion of the zygomatic arch was replaced by fibrous tissue containing spicules of bone and necrotic debris. Because the masseter is a crucial muscle for moving the jaw, it is likely that the nutritional status of the mice was adversely affected by the zygomatic arch fractures. Consistent with this idea, the plasma glucose and total protein levels tended to be lower in the *Zmpste24*$^{-/-}$ mice (Table 1). The μCT scans of 2- to 3-month-old mice also revealed striking micrognathia and a reduction in the zig-zag appearance of the cranial sutures. The micrognathia may have been secondary to the zygomatic arch fractures, as the zygomatic arch was usually normal at 18 days of age, and the size and shape of the mandible were fairly normal (not shown).

The thoracic vertebrae of each *Zmpste24*$^{-/-}$ mouse had reduced bone density compared with *Zmpste24*$^{+/+}$ controls. This was very obvious from the three-dimensional μCT reconstructions of the vertebral column (surface renderings generated at the same threshold), which showed the vertebral bodies from *Zmpste24*$^{-/-}$ mice ($n = 4$) to be more porous ("pock-marked") than those of *Zmpste24*$^{+/+}$ controls ($n = 5$) (Fig. 3*e*). The pock-marked areas identify regions of bone with a density below the threshold level. The three-dimensional analysis of trabecular bone within the 12th vertebral body revealed that the ratio of bone volume to the total volume was reduced by 34% in the *Zmpste24*$^{-/-}$ mice ($P = 0.04$). The thickness of the trabeculae in the vertebrae was reduced by 36% ($P = 0.02$). An increase in pock marking of bone was also evident in the lower extremities (note the proximal fibula in the *Zmpste24*$^{-/-}$ mouse) (Fig. 3*f*). To quantify bone abnormalities in this predominantly cortical area, we calculated the ratio of *bone* volume in the tibia and fibula to *total* volume of those bones. This ratio was lower in *Zmpste24*$^{-/-}$ mice (0.54 ± 0.09) than in littermate *Zmpste24*$^{+/+}$ mice (0.67 ± 0.03, $P = 0.02$), which means that even when the values are corrected for bone size, there is thinner cortical bone in the *Zmpste24*$^{-/-}$ mice. We suspect that there might be a bone abnormality in heterozygous mice as well. We performed μCT scans on two 15-month-old heterozygous *Zmpste24* knockout mice (exhibiting alopecia and weight loss) and age-matched *Zmpste24*$^{+/+}$ controls and identified degraded transverse and spinous processes in the thoracic and lumbar vertebrae of the heterozygotes (not shown).

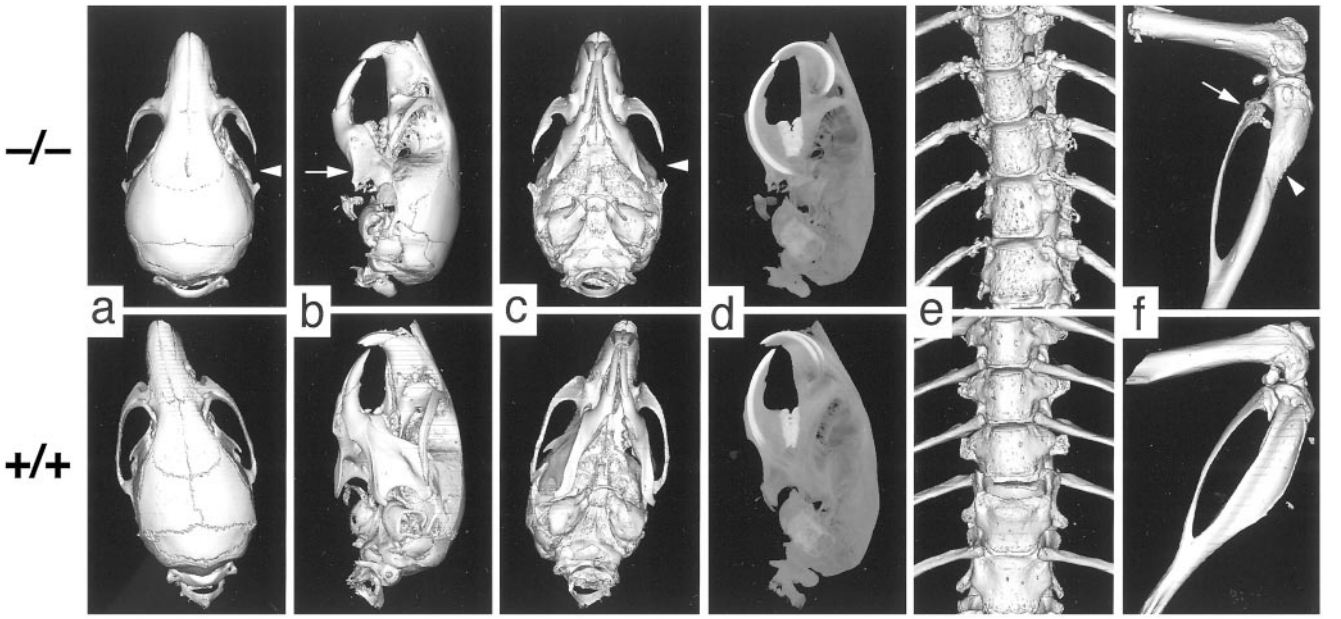

Fig. 3. μCT scans illustrating bony lesions in *Zmpste24*$^{-/-}$ mice. (*a–c*) Surface renderings of top, lateral, and bottom surfaces of the skulls of 8-week-old *Zmpste24*$^{-/-}$ and *Zmpste24*$^{+/+}$ mice. Arrowheads indicate the destroyed zygomatic arch in *a* and *c*; an arrow indicates the small mandible in *b*. (*d*) Maximal intensity projection of the lateral view of the skulls of 8-week-old mice, revealing an increase in the length of the incisors and the size of other teeth. (*e*) Surface rendering of the thoracic spines of 8-week-old *Zmpste24*$^{-/-}$ and *Zmpste24*$^{+/+}$ mice, revealing increased numbers of pock marks in the *Zmpste24*$^{-/-}$ mice. (*f*) Surface rendering of the femur, knee, tibia/fibula of 2-month-old *Zmpste24*$^{-/-}$ and *Zmpste24*$^{+/+}$ mice, revealing increased pock marks in the proximal fibula of the *Zmpste24*$^{-/-}$ mouse as well as effacement of the tibial tuberosity.

The bone abnormalities in *Zmpste24*$^{-/-}$ mice were not accompanied by perturbations in the plasma levels of calcium or phosphate (Table 1). *Zmpste24*$^{-/-}$ mice did not manifest evidence of increased bone turnover. *Zmpste24*$^{-/-}$ mice had lower alkaline phosphatase levels. Urinary levels of deoxypyridinoline, a bone collagen breakdown product (21), were not different in *Zmpste24*$^{-/-}$ and *Zmpste24*$^{+/+}$ mice. Also, bones from *Zmpste24*$^{-/-}$ and *Zmpste24*$^{+/+}$ mice contained similar numbers of osteoclasts, as judged by staining for tartrate-resistant acid phosphatase (not shown).

Gait and Grip Abnormalities. *Zmpste24*$^{-/-}$ mice also exhibited a slow hobbling gait, frequently dragging their hind limbs (Fig. 4). We suspect that the muscle weakness in the lower extremity contributed to the marked effacement of the anterior tibial tuberosity (the origin of the tibialis anterior muscle) (Fig. 3*f*). In addition, *Zmpste24*$^{-/-}$ mice ($n = 11$) were able to hang onto a grid after it was turned upside down for only a few seconds [males, 3.0 ± 1.5 s ($n = 8$); females, 4.5 ± 5.3 s ($n = 6$)], whereas littermate *Zmpste24*$^{+/-}$ and *Zmpste24*$^{+/+}$ mice ($n = 12$ males; $n = 13$ females) were able to hold on almost indefinitely (>45 s). We examined muscles throughout the limbs and trunk of *Zmpste24*$^{-/-}$ mice. Despite exhaustive analysis of hematoxylin- and eosin-stained material, we identified no abnormalities in the skeletal muscle fibers of *Zmpste24*$^{-/-}$ mice (Fig. 5*a*). Further specialized neuromuscular studies are warranted to define the nature of the muscular defect in *Zmpste24*$^{-/-}$ mice.

Table 1. Plasma and urine chemistries in *Zmpste24*$^{-/-}$ mice

	Zmpste24$^{+/+}$	*Zmpste24*$^{-/-}$
Glucose, mg/dl	191 ± 61	176 ± 77
Total protein, g/dl	6.7 ± 1.0	5.8 ± 2.8
Alanine aminotransferase, units/liter	61 ± 37	44 ± 32
Aspartate aminotransferase, units/liter	141 ± 71	120 ± 83
Alkaline phosphatase, units/liter	83 ± 9	59 ± 9*
Calcium, mmol/liter	9.22 ± 0.67	9.64 ± 0.70
Phosphate, mmol/liter	7.84 ± 4.47	9.78 ± 4.02
Urinary deoxypyridinoline, nmol/mg creatinine (14-week-old mice)	0.22 ± 0.04	0.25 ± 0.03
Urinary deoxypyridinoline, nmol/mg creatinine (4-week-old mice)	0.21 ± 0.03	0.21 ± 0.04

Data are presented as mean and SD; $n = 6–10$ adult mice per group, ages 15–24 weeks except as indicated. *, $P < 0.01$. Except for alkaline phosphatase, no differences were significant ($P > 0.05$).

Prelamin A Processing Defect. The inability to hold onto a grid while upside down is identical to a phenotype in mice lacking prelamin A (22). Accordingly, we examined prelamin A processing in *Zmpste24*$^{-/-}$ fibroblasts and found clear-cut abnormalities. Western blots of *Zmpste24*$^{-/-}$ fibroblast extracts with an antibody against the C terminus of prelamin A revealed a striking accumulation of prelamin A (Fig. 6). Western blots with an antibody against the N terminus of lamin A revealed fully

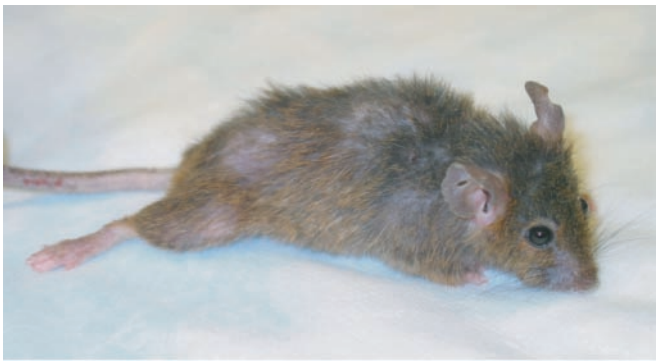

Fig. 4. Photograph of a *Zmpste24*$^{-/-}$ mouse, illustrating a characteristic dragging of the hind limb.

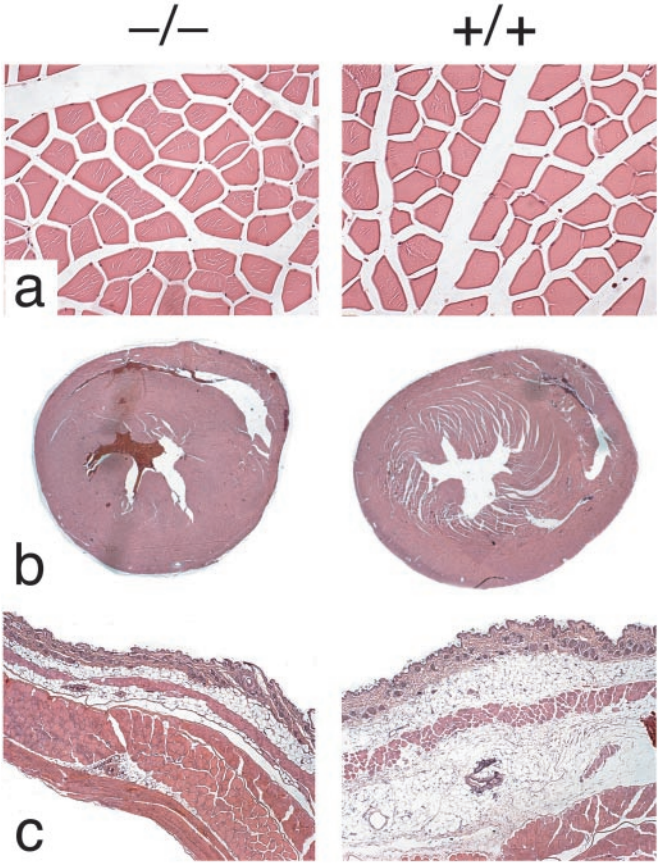

Fig. 5. (*a*) Paravertebral muscles from 19-week-old male *Zmpste24*$^{-/-}$ and Zmpste24$^{+/+}$ mice. (*b*) Sections through the hearts of 19-week-old male *Zmpste24*$^{-/-}$ and *Zmpste24*$^{+/+}$ mice. (*c*) Sections through the skin of 15-week-old female *Zmpste24*$^{-/-}$ and Zmpste24$^{+/+}$ mice, showing reduced adipose tissue in *Zmpste24*$^{-/-}$ mice.

processed lamin A (72 kDa) in *Zmpste24*$^{+/+}$ fibroblasts and a larger unprocessed prelamin A (74 kDa) in *Zmpste24*$^{-/-}$ fibroblasts (Fig. 6). These findings are identical to those in a very recent paper by Pendás *et al.* (12). We asked whether prelamin A might accumulate in fibroblasts lacking the *CAAX* methyltransferase Icmt (15) or the *CAAX* endoprotease Rce1 (14). Interestingly, prelamin A accumulated in *Icmt*$^{-/-}$ but not in *Rce1*$^{-/-}$ fibroblasts (Fig. 6). As predicted from earlier studies (10), a farnesyltransferase inhibitor blocked prelamin A processing (Fig. 6).

Given that *CAAX* endoproteolysis (i.e., removal of the *−AAX*) is required for carboxyl methylation by Icmt, we are forced to conclude that the release of the *−AAX* from prelamin A can proceed in the absence of Rce1. Because Ste24p can release the *−AAX* from a-factor, it seems reasonable to presume that Zmpste24 is capable of releasing the *−AAX* from prelamin A. The results with the *Rce1*$^{-/-}$ fibroblasts are intriguing because they are the first to suggest that a protease aside from Rce1 can remove the *−AAX* from a mammalian *CAAX* protein (6, 14, 23).

We do not yet know the precise role of Zmpste24 in prelamin A processing. An attractive possibility is that Zmpste24 carries out both prelamin A processing steps (the release of the *−AAX* and the release of the additional 15 residues), just as Ste24p has dual functions in a-factor biogenesis. On the other hand, it is possible that the only role of Zmpste24 is clipping the *−AAX*, allowing methylation to proceed. We do not yet know whether Rce1 retains the capacity to cleave the *−AAX* from prelamin A in *Zmpste24*$^{+/+}$ cells. If Rce1 lacks that ability, one would be forced to consider the possibility that Zmpste24's only role in prelamin A processing is to release the *−AAX*, leaving the second proteolytic processing step to another enzyme. Consistent with the latter possibility are reports that the second prelamin A proteolytic processing step is carried out by a serine protease located in the cell nucleus (10, 24). [Zmpste24 is a zinc metalloproteinase, not a serine protease (1–3).] Additional biochemical and genetic studies over the next few years will undoubtedly define the precise role(s) of Zmpste24 in lamin A biogenesis.

The muscle weakness in *Zmpste24*$^{-/-}$ mice seems consistent with a defect in prelamin A processing (22, 25), but it is unclear whether the prelamin A processing defect lies at the root of the osteogenesis imperfecta-like phenotype. Osteogenesis imperfecta is an autosomal dominant syndrome generally caused by mutations in the type I procollagen genes. Most commonly, the procollagen mutations result in reduced amounts of type I

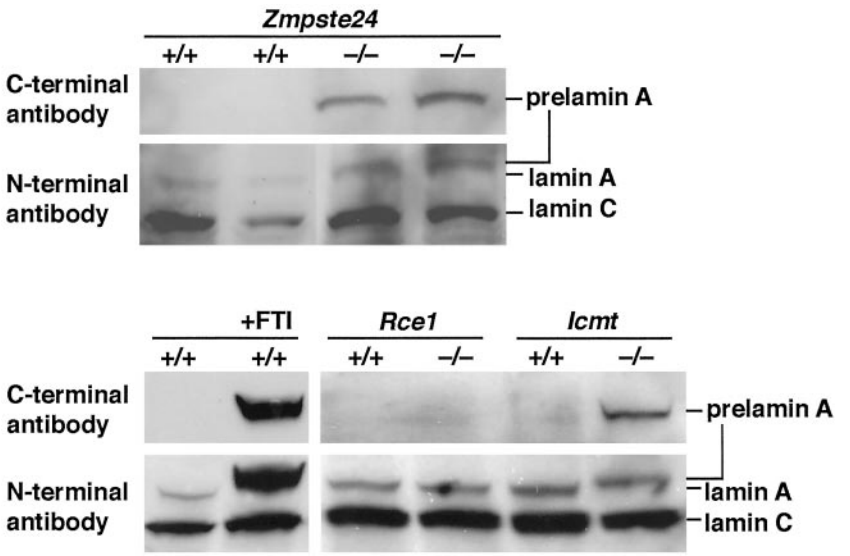

Fig. 6. Western blots of *Zmpste24*$^{-/-}$, *Icmt*$^{-/-}$, and *Rce1*$^{-/-}$ fibroblast extracts with a C-terminal prelamin A antibody and an N-terminal lamin A/C antibody. Also shown are Western blots of extracts of wild-type fibroblasts and fibroblasts treated with 5 μM SCH66336, a farnesyltransferase inhibitor.

procollagen secretion, but some mutations result in the secretion of a structurally abnormal procollagen (17). One possibility is that the prelamin A accumulation in the nuclear envelope of *Zmpste24*$^{-/-}$ mice indirectly affects the amount or quality of type I procollagen secretion, accounting for the bone phenotype in *Zmpste24*$^{-/-}$ mice. Somewhat against this possibility, although, is the fact that a heightened susceptibility to bone fractures has never been identified in humans with lamin A mutations. Another obvious possibility is that Zmpste24 has additional protein substrates and that defective processing of those additional substrates causes the bone abnormality. The fact that Zmpste24 might have additional substrates is not farfetched, as *Zmpste24* orthologs clearly exist in organisms that lack type A nuclear lamins (e.g., yeast and nematodes). Also, *STE24* mutations in yeast reverse the topological orientation of certain membrane proteins (7), and the stability of several misfolded proteins retained in the endoplasmic reticulum is enhanced in *ste24*Δ yeast (S.M. and Claude Jakob, unpublished observations). Both of the latter observations suggest that Ste24p could be required, directly or indirectly, in the recognition and removal of misfolded proteins within the endoplasmic reticulum. If *Zmpste24* deficiency in mice were to interfere with the recognition and/or degradation of misfolded type I procollagen molecules, it is easy to imagine how an osteogenesis imperfecta-like syndrome might occur.

Comparisons with a Second Line of *Zmpste24*$^{-/-}$ Mice. Very recently, Pendás *et al.* (12) characterized a second line of *Zmpste24*$^{-/-}$ mice. A large number of similarities (abnormal growth curves, early death, loss of fur, kyphosis, abnormal gait, muscle weakness, normal or low plasma glucose levels, and abnormal prelamin A processing) indicate that our *Zmpste24*$^{-/-}$ mice and theirs are fundamentally the same. However, there were some differences in our reports. Pendás *et al.* (12) claimed that their mice exhibited a "growth plate dysplasia" in the femur and tibia, although they did not show data. The growth plates of the femur and tibia in our mice were normal. They did not uncover a bone fracture phenotype, which can easily be overlooked unless one specifically looks for it. They reported that heterozygotes were healthy, whereas we found that older heterozygotes lose weight and develop alopecia. They also reported that their mice had a lamin A-related cardiomyopathy with thinning of the ventricles and secondary liver disease. Over the past 3 years, we have looked assiduously for heart or liver pathology over the life span of *Zmpste24*$^{-/-}$ mice, but have found none. Our *Zmpste24*$^{-/-}$ mice did not have ventricular thinning (Fig. 5*b*) nor did they have myocardial fibrosis as assessed by trichrome staining (not shown). Also, the plasma levels of alanine aminotransferase and aspartate aminotransferase were not elevated in our *Zmpste24*$^{-/-}$ mice (Table 1). Finally, they found reduced adipose tissue in *Zmpste24*$^{-/-}$ mice and concluded that they had a lamin A-related partial lipodystrophy. Subcutaneous adipose tissue was invariably reduced in our *Zmpste24*$^{-/-}$ but was always detectable, even in old and debilitated mice (Fig. 5*c*). It is possible that *Zmpste24*$^{-/-}$ mice do have a lamin A-related partial lipodystrophy, but in view of the low-normal glucose levels in our mice (Table 1) and the normal or low glucose and triglyceride levels in their mice, we suspect that the reduced fat stores may have had more to do with starvation secondary to the bone abnormalities (i.e., complete destruction of the zygomatic arch and other bone fractures limiting access to food).

We thank M. Sinensky for advice, R. Bishop (Schering–Plough, Kenilworth, NJ) for SCH66336, and S. Bergö for assistance with statistics. This work was supported in part by National Institutes of Health Grants HL41633 and AG15451 (to S.G.Y.) and GM41223 (to S.M.), by grants from the University of California Tobacco-Related Disease Research Program (to M.O.B. and S.G.Y.), and by the Swedish Cancer Foundation (to M.O.B.).

1. Fujimura-Kamada, K., Nouvet, F. J. & Michaelis, S. (1997) *J. Cell Biol.* **136,** 271–285.
2. Tam, A., Nouvet, F. J., Fujimura-Kamada, K., Slunt, H., Sisodia, S. S. & Michaelis, S. (1998) *J. Cell Biol.* **142,** 635–649.
3. Boyartchuk, V. L., Ashby, M. N. & Rine, J. (1997) *Science* **275,** 1796–1800.
4. Boyartchuk, V. L. & Rine, J. (1998) *Genetics* **150,** 95–101.
5. Hrycyna, C. A., Sapperstein, S. K., Clarke, S. & Michaelis, S. (1991) *EMBO J.* **10,** 1699–1709.
6. Young, S. G., Ambroziak, P., Kim, E. & Clarke, S. (2000) in *The Enzymes*, eds. Tamanoi, F. & Sigman, D. S. (Academic, San Diego), Vol. 21, pp. 155–213.
7. Tipper, D. J. & Harley, C. A. (2002) *Mol. Biol. Cell* **13,** 1158–1174.
8. Tong, A. H. Y., Evangelista, M., Parsons, A. B., Xu, H., Bader, G. D., Pagé, N., Robinson, M., Raghibizadeh, S., Hogue, C. W. V., Bussey, H., *et al.* (2001) *Science* **294,** 2364–2368.
9. Leung, G. K., Schmidt, W. K., Bergo, M. O., Gavino, B., Wong, D. H., Tam, A., Ashby, M. N., Michaelis, S. & Young, S. G. (2001) *J. Biol. Chem.* **276,** 29051–29058.
10. Kilic, F., Dalton, M. B., Burrell, S. K., Mayer, J. P., Patterson, S. D. & Sinensky, M. (1997) *J. Biol. Chem.* **272,** 5298–5304.
11. Olson, E. N., Arnold, H.-H., Rigby, P. W. J. & Wold, B. J. (1996) *Cell* **85,** 1–4.
12. Pendás, A. M., Zhou, Z., Cadiñanos, J., Freije, J. M. P., Wang, J., Hultenby, K., Astudillo, A., Wernerson, A., Rodríguez, F., Tryggvason, K. & Lopéz-Otín, C. (2002) *Nat. Genet.* **31,** 94–99.
13. Lewandoski, M. & Martin, G. R. (1997) *Nat. Genet.* **17,** 223–225.
14. Kim, E., Ambroziak, P., Otto, J. C., Taylor, B., Ashby, M., Shannon, K., Casey, P. J. & Young, S. G. (1999) *J. Biol. Chem.* **274,** 8383–8390.
15. Bergo, M. O., Leung, G. K., Ambroziak, P., Otto, J. C., Casey, P. J., Gomes, A. Q., Seabra, M. C. & Young, S. G. (2001) *J. Biol. Chem.* **276,** 5841–5845.
16. Pereira, R., Khillan, J. S., Helminen, H. J., Hume, E. L. & Prockop, D. J. (1993) *J. Clin. Invest.* **91,** 709–716.
17. Byers, P. H. (2001) in *The Metabolic and Molecular Bases of Inherited Disease*, eds. Scriver, C. R., Beaudet, A. L., Sly, W. S., Valle, D., Childs, B., Kinzler, K. W. & Vogelstein, B. (McGraw–Hill, New York), Vol. 4, pp. 5241–5285.
18. Stacey, A., Bateman, J., Choi, T., Mascara, T., Cole, W. & Jaenisch, R. (1988) *Nature (London)* **332,** 131–136.
19. Bonadio, J., Saunders, T. L., Tsai, E., Goldstein, S. A., Morris-Wiman, J., Brinkley, L., Dolan, D. F., Altschuler, R. A., Hawkins, J. E., Jr., Bateman, J. F., *et al.* (1990) *Proc. Natl. Acad. Sci. USA* **87,** 7145–7149.
20. Forlino, A., Porter, F. D., Lee, E. J., Westphal, H. & Marini, J. C. (1999) *J. Biol. Chem.* **274,** 37923–37931.
21. Cahoon, S., Boden, S. D., Gould, K. G. & Vailas, A. C. (1996) *J. Med. Primatol.* **25**, 333–338.
22. Sullivan, T., Escalante-Alcalde, D., Bhatt, H., Anver, M., Bhat, N., Nagashima, K., Stewart, C. L. & Burke, B. (1999) *J. Cell Biol.* **147,** 913–919.
23. Otto, J. C., Kim, E., Young, S. G. & Casey, P. J. (1999) *J. Biol. Chem.* **274,** 8379–8382.
24. Kilic, F., Johnson, D. A. & Sinensky, M. (1999) *FEBS Lett.* **450,** 61–65.
25. Brown, C. A., Lanning, R. W., McKinney, K. Q., Salvino, A. R., Cherniske, E., Crowe, C. A., Darras, B. T., Gominak, S., Greenberg, C. R., Grosmann, C., *et al.* (2001) *Am. J. Med. Genet.* **102,** 359–367.